



The 2019 flash droughts in subtropical eastern Australia and their association with large-scale climate drivers

Hanh Nguyen^{a,*}, Matthew C. Wheeler^a, Harry H. Hendon^a, Eun-Pa Lim^a, Jason A. Otkin^b

^a Bureau of Meteorology, Melbourne, Australia

^b Space Science and Engineering Center, Cooperative Institute for Meteorological Satellite Studies, University of Wisconsin-Madison, USA

ARTICLE INFO

Keywords:

Flash drought
Evaporative stress index
Subtropical eastern Australia
Predictability
Climate drivers

ABSTRACT

During 2017–2019, drought existed in many parts of Australia with varying degrees of severity and varied timing of development and intensification. In a broad sense, the surface climate conditions went from anomalously wet in 2016 to an official government-declared drought from the end of 2017. The drought subsequently intensified further to become most severe in mid to late 2019. Here we explore the more detailed evolution of the 2019 conditions over subtropical eastern Australia and infer its predictability through linear relationships with large-scale climate drivers. To monitor the detailed drought evolution, we use the Evaporative Stress Index (ESI) computed over a 4-week running window on a 5 km grid. Flash drought onset is defined as when there is a rapid decline in the ESI that is sustained over at least 2 weeks which ends in drought conditions. For the Central Slopes area of the upper Darling River basin, flash drought onset occurred in June, persisted over 6 months, and rapidly terminated through a flash recovery in February 2020. In the far east of Australia (East Coast regions), flash drought onset was identified later, in November and December. For the Central Slopes area, less than half the magnitude of the flash drought development in June could be explained through linear relationships with the positive Indian Ocean Dipole mode (IOD) and the central Pacific El Niño, together with the long-term trend in ESI in the region. Similarly, only about half the magnitude of the East Coast flash drought developments in November and December could be explained by the ongoing positive IOD, central Pacific El Niño, negative Southern Annular Mode, and ongoing global warming trend. Therefore, although these large-scale drivers set the stage for the likelihood of drought, successful prediction of flash drought will require more local and current information than those large-scale climate drivers alone.

1. Introduction

Beginning in early 2017 and extending to the end of 2019, subtropical eastern Australia, including the agriculturally-important Murray Darling Basin (MDB) and the densely populated East Coast regions (MDB, ECS and ECN in Fig. 1a), experienced hydrological drought due to large rainfall deficits (Bureau's [Special Climate Statement 70, 2019](#); see also the Bureau's drought report webpage <http://www.bom.gov.au/climate/drought/>). The 2017–2019 drought also affected most of the state of New South Wales and southern Queensland. The rainfall deficits were especially sustained during 2018–19. For example, in the Central Slopes (CS) area of the north-eastern MDB (Fig. 1b) there were only three months of at least normal precipitation during those 2 years and the 36-month period 2017–2019 was the driest on record (more than 100 mm lower than the next driest period of 1965–67). The dryness

was particularly concentrated during the cool season (April–September), which is the most important season in much of southern Australia for recharging soil moisture and generating runoff. The accumulated April–September rainfall totals over subtropical eastern Australia for each of 2017, 2018, and 2019 were among the 10 lowest years on record since 1901 when observation data became available. Each of these years had rainfall totals that were at least 50% below the 1961–1990 average, which is an unprecedented sequence of unusually dry years. The very much below average October and November rainfall in 2019 over most of the main water catchments of subtropical eastern Australia further exacerbated the effect of low inflows during the prior years. The catchment average soil moisture over the 3-year period was the lowest on record in ten of the 26 river catchments in the MDB (Bureau's [Special Climate Statement 70, 2019](#)). These years were also the warmest on record with maximum temperature anomalies for

* Corresponding author. Bureau of Meteorology, 700 Collins Street, Docklands, VIC, 3008, Australia.

E-mail address: hanh.nguyen@bom.gov.au (H. Nguyen).

<https://doi.org/10.1016/j.wace.2021.100321>

Received 6 October 2020; Received in revised form 26 February 2021; Accepted 7 April 2021

Available online 12 April 2021

2212-0947/Crown Copyright © 2021 Published by Elsevier B.V. This is an open access article under the CC BY-NC-ND license

(<http://creativecommons.org/licenses/by-nc-nd/4.0/>).

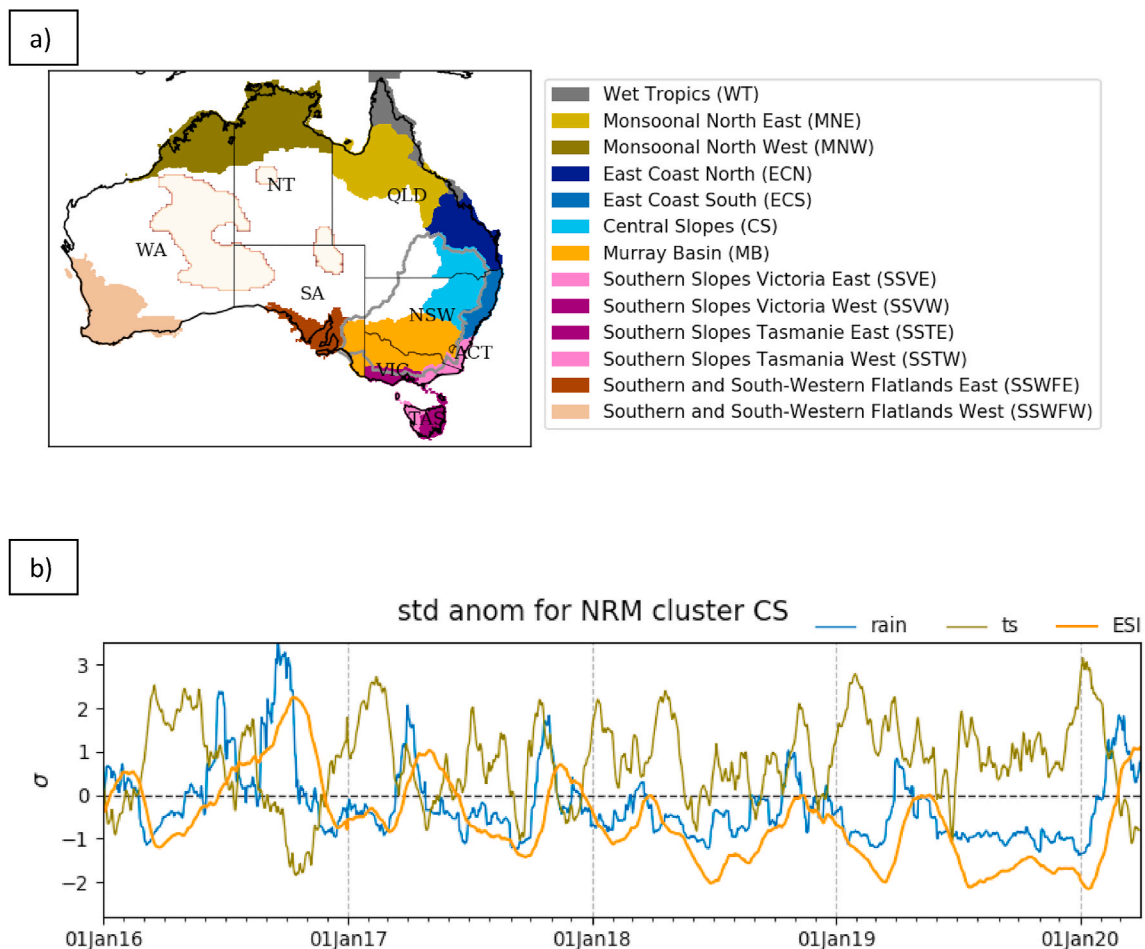


Fig. 1. (a) Map showing the thirteen clusters of natural resource management (NRM) regions using a unique Australian regionalisation scheme taken from <https://www.climatechangeinaustralia.gov.au/en/climate-projections/about/modelling-choices-and-methodology/regionalisation-schemes/>. The grey contour indicates the Murray-Darling basin (MDB). The six states and two territories are indicated on the map by their acronyms: Western Australia (WA), Northern Territory (NT), Queensland (QLD), South Australia (SA), New South Wales (NSW), Victoria (VIC) and Australian Capital City (ACT) and Tasmania (TAS). The light beige regions encircled by the brown contours indicate where there is insufficient observational data to reliably compute the ESI and is therefore masked out. (b) Time series of the ESI (orange) and rainfall (blue) and 2-m temperature (olive) anomalies averaged over the NRM cluster CS. The anomalies were normalized by their respective standard deviation. Note that the date refers to the end of the 4-week window over which the ESI, rainfall, and temperature are averaged. Time marks are placed on the 1st day of each month. (For interpretation of the references to colour in this figure legend, the reader is referred to the Web version of this article.)

subtropical eastern Australia reaching 1.73 °C, 1.91 °C and 2.13 °C above the 1961–1990 average of 24.9 °C, respectively.

Although the cause of the low rainfall during 2017 and 2018 is still being debated, the extreme dryness during 2019 has been attributed to the occurrence of a record positive Indian Ocean Dipole (IOD) (Bureau special climate statement 70) along with strong El Niño Modoki (Lim et al., 2021), both of which are known to act to reduce rainfall in subtropical eastern Australia during the cool season (Wang and Hendon 2007; Cai et al., 2012). In addition, a rare strong Southern Hemisphere polar stratospheric warming occurred at the beginning of September 2019, which subsequently promoted a strong negative polarity of the Southern Annular Mode (SAM) from late October through to the end of December 2019 (Lim et al., 2021). Low SAM in response to polar stratospheric warmings has been shown to promote hot and dry conditions and bushfires across subtropical eastern Australia in austral late spring to early summer (Lim et al. 2019, 2021).

The purpose of the present study is to investigate the exacerbation of the drought during 2019 from the perspective of evaporative stress as monitored by the Evaporative Stress Index (ESI), which is an integrated metric that captures the combined influence of multiple factors contributing to drought such as soil moisture deficit and elevated evaporative demand. The ESI is more indicative of drought conditions

that affect agriculture and natural ecosystems than, for instance, the rainfall deficiency, as it can better capture the factors that contribute to the total stress on vegetation. Nguyen et al. (2020) showed that the 2017–2019 drought in subtropical eastern Australia was associated with above normal evaporative stress (i.e. negative ESI). Nguyen et al. (2019) also demonstrated the utility of the ESI for identifying flash drought in Australia as per the definition of Otkin et al. (2018a,b). Flash drought, which refers to drought that rapidly develops or intensifies within a few weeks, is especially important for some agricultural practices because the rapid intensification can have dire consequences for plant survival and production (e.g., Nguyen et al., 2019; Otkin et al., 2018a,b). We therefore use the ESI to study in detail the development of the drought during 2019, identifying occurrences of flash drought, and attempt to attribute their cause and infer their predictability.

The paper is organised as follows: The data and methods are described in section 2. Details of the 2017–2019 multi-year drought and its evolution during 2019 are described in section 3. The role of large-scale climate drivers on the life cycle of the 2019 flash drought and its inferred predictability are investigated in section 4, and the conclusion is given in section 5.

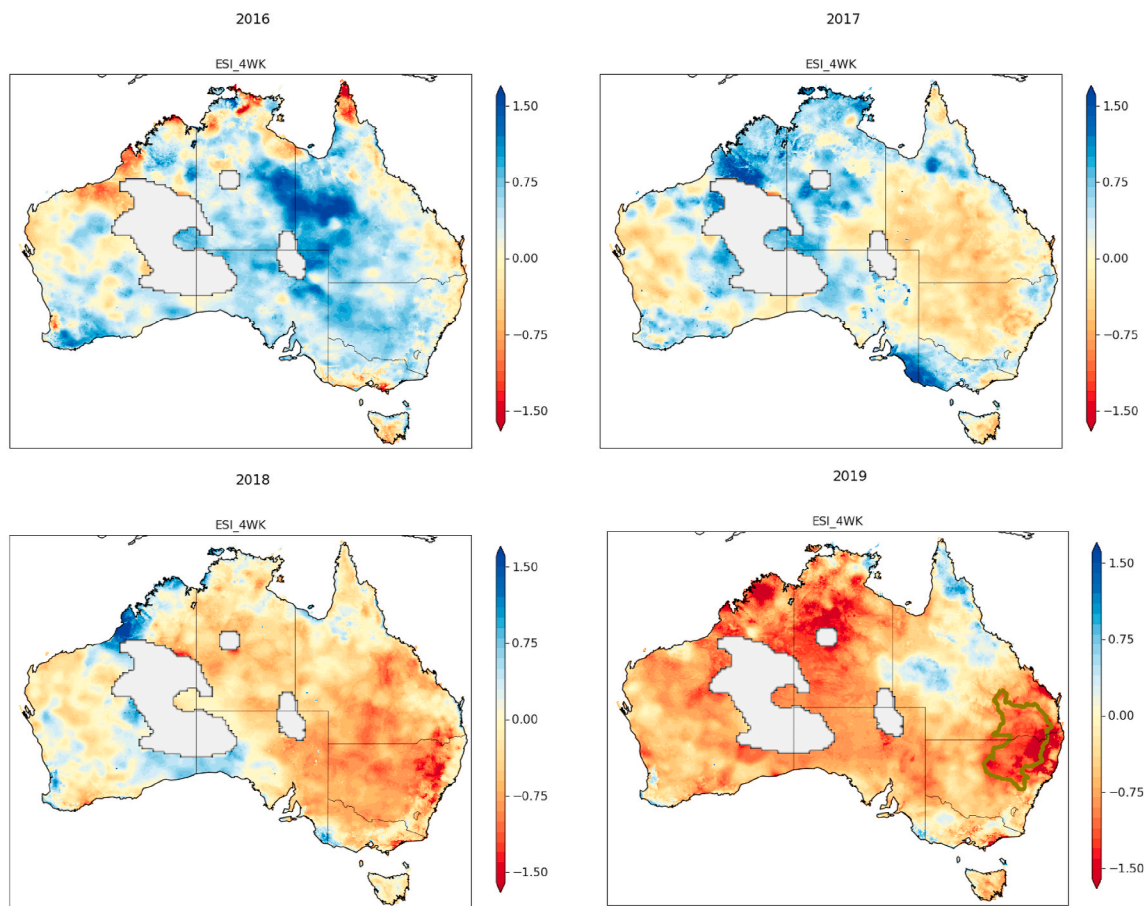


Fig. 2. Annual mean ESI for Australia for 2016 to 2019. The green contour on the 2019 map indicates the NRM cluster CS which coincide with the epicentre of strongest negative ESI. (For interpretation of the references to colour in this figure legend, the reader is referred to the Web version of this article.)

2. Data and method

This study uses the daily analyses of precipitation and surface air temperature from the Australian Water Availability Project (AWAP, Jones et al., 2009). These analyses are based on an optimum interpolation of available station observations and are provided on a 5 km grid. The analyses are performed daily for 1900-present. We also use some of the output from version 6 of the Bureau of Meteorology’s land surface landscape water-balance model (AWRA-L v6, Frost et al., 2018) to assess the drought evolution. The one-dimensional water balance model produces daily outputs on a 5 km grid that include evapotranspiration (ET) and potential ET (PET), which are used to compute the ESI. ET in the AWRA-L model is estimated as the sum of evaporation (interception, soil and groundwater) and transpiration (shallow and deep root water uptake and transpiration from groundwater). PET in the AWRA-L model is computed using the Penman equation (Penman 1948) as a combination of net radiation and vapour pressure deficit, and is indicative of the demand for moisture from the atmosphere. Validation against independent observation (mainly stream flow) and comparison to other model-derived analyses indicate that AWRA-L provides good estimates of ET (Khan et al., 2020). The AWRA-L model is driven with observed inputs of rainfall, temperature, solar radiation and wind speed to estimate ET and PET. Therefore, the ET and PET are observation-constrained and not purely model based. AWRA-L outputs are available in near real-time and extend back to 1911.

The ESI is the standardized anomaly of the ratio ET/PET. Agricultural drought is implied by strongly negative values of the ESI, when actual ET is reduced due to lack of available moisture in the soil and PET is increased due to factors such as increased air temperature and wind

speed. Normalizing ET anomaly by PET serves to remove some of the variability in ET due to seasonal variations in available energy and vegetation cover amount (e.g., Anderson et al., 2013). In this study the ESI is computed daily over a 4-week window, with the last day of the window being the date of that window, using the climatology from 1975 to 2018. Quantities are also defined to measure changes in the ESI. More precisely, the quantities calculated are:

- (i) The ESI computed at each time step t as:

$$ESI(t) = \frac{r_{ET(t)} - \langle r_{ET}(t_{clim}) \rangle}{\sigma(r_{ET}(t_{clim}))}$$

where $r_{ET} = \frac{ET}{PET}$, and $\langle r_{ET}(t_{clim}) \rangle$ and $\sigma(r_{ET}(t_{clim}))$ are its climatological mean and standard deviation, respectively, for time t of the year computed over the period 1975–2018.

- (ii) Changes in the ESI over a 2-week interval (δESI) are used to capture the rapid intensification of drought. The 2-week interval is chosen to avoid short-lived dry spells that may lead to a false alarm of onset of flash drought (Christian et al., 2019). Like the ESI, the change anomalies are standardized by the standard deviation of the same 2 week change in the climatological period:

$$\delta ESI(t) = \frac{dESI(t) - \langle dESI(t_{clim}) \rangle}{\sigma(dESI(t_{clim}))}$$

where $dESI(t) = ESI(t) - ESI(t - 2wk)$ is the ESI difference between the 2-week intervals, and $\langle dESI(t_{clim}) \rangle$ and $\sigma(dESI(t_{clim}))$ are its climatological mean and standard deviation for the time of the year t , respectively.

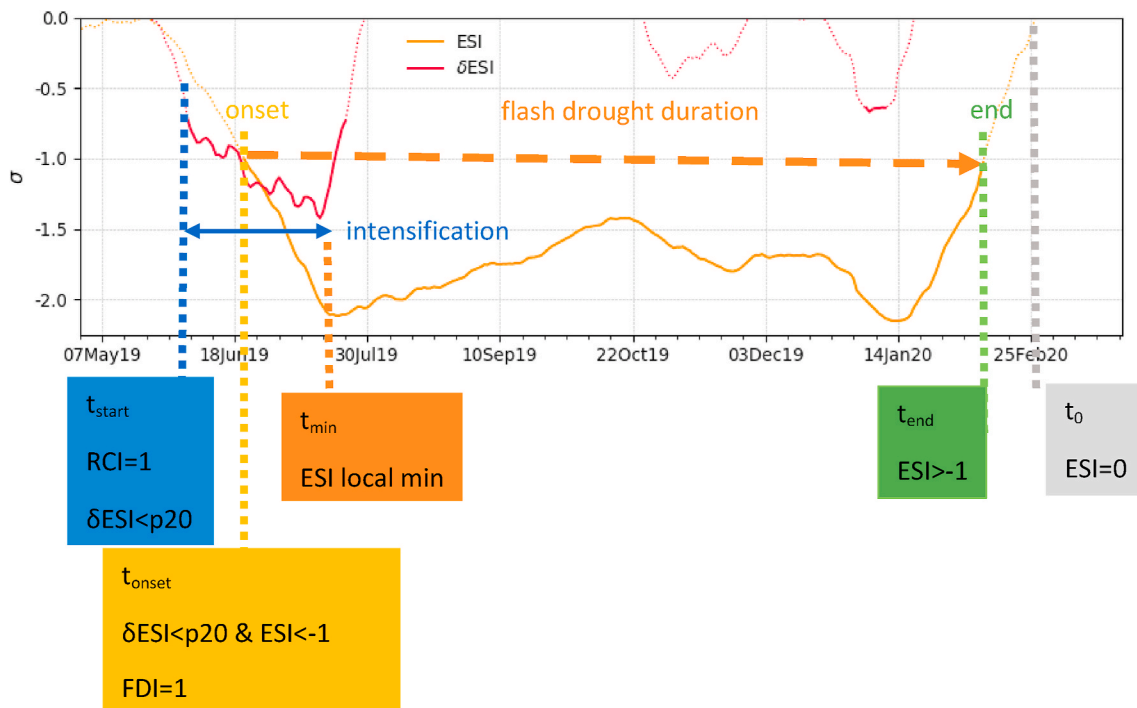


Fig. 3. Schematic of flash drought monitoring using the ESI (orange with values ≤ -1 bold) and δESI (dashed magenta with values below the 20th percentile bold). Four different stages are indicated: t_{start} is the first instance $RCI=1$, t_{onset} is the onset of when ESI drops below -1 , thereby representing the onset of the event, t_{min} is the ESI local minimum indicating the end of the intensification period, t_{end} is when the ESI becomes > -1 , thereby representing the end of the event and t_0 is when ESI reaches 0 marking the return to normal conditions. Time marks are placed every 7 days. (For interpretation of the references to colour in this figure legend, the reader is referred to the Web version of this article.)

(iii) The Rapid Change Index (RCI) at each time step t is used to capture the intensification phase of a potential flash drought event when δESI is below its 20th percentile ($p20$). $p20$ is a single value estimated for each individual region over the full data period for this study (1975–2020). RCI is set to 1 when δESI is below $p20$ and set to 0 otherwise:

$$RCI(t) = \begin{cases} 1, & \delta ESI \leq p20 \\ 0, & \delta ESI > p20 \end{cases}$$

(iv) The Flash Drought Index (FDI) at each time step t is used to detect the onset of a potential flash drought event. Flash drought is defined to occur when $RCI = 1$ for a sequence of at least 2 weeks and the ESI is less than -1 (i.e., drought, Nguyen et al., 2020) at the end of the 2-week period. This definition ensures that the rapid intensification occurs over at least 2 weeks (Otkin et al., 2018a,b; Pendergrass et al., 2020) and that the end point for the period of change is in drought condition:

$$FDI(t) = \begin{cases} 1, & \text{if } RCI(t) = 1 \text{ for at least 2 weeks and } ESI(t) \leq -1 \\ 0, & \text{otherwise} \end{cases}$$

Global analysis of Reynolds daily sea surface temperature (SST) is used to investigate potential relationships of SST anomalies with the ESI. These SST data are the National Oceanic and Atmospheric Administration (NOAA)’s optimum interpolation SST that is based on a combination of remotely sensed ocean temperatures from satellite and in situ observations and is interpolated globally to a 0.25° resolution grid that spans from 1982 to present (Reynolds et al., 2007). Computation of daily indices of the Indian Ocean Dipole Mode Index (DMI) and the central Pacific El Niño Modoki index (EMI) is performed using the daily SST,

and then averaged over a daily running window of 4 weeks to be compatible with the ESI. The DMI^1 is defined as the difference in SST between boxes in the eastern and the western Indian Ocean as defined by Saji et al. (1999). The EMI^2 is the difference in SST between the three equatorial Pacific regions as defined by Ashok et al. (2007) and captures El Niño variations that occur near the dateline as opposed to those that occur in the eastern equatorial Pacific. Daily SAM is monitored by the Antarctic Oscillation (AAO³) index (SAMI), which was retrieved from the NOAA National Weather Service webpage (https://www.cpc.ncep.noaa.gov/products/precip/CWlink/daily_ao_index/ao/ao.shtml).

With the aim to attribute the cause and predictability of the 2019 drought evolution, we reconstruct the ESI via multiple linear regression using four predictors: de-trended and standardized EMI, DMI and SAMI, and time that depicts the long-term linear trend in ESI. The first three indices capture the key modes of monthly to interannual variability of the climate system that most strongly affect Australian rainfall (e.g., Risbey et al., 2009). We include the trend to capture possible effects of ongoing global warming on evaporative stress. We do not expect a primary contribution of the trend to the evaporative stress because we previously found the trends in ESI to be relatively small and/or of mixed sign in subtropical eastern Australia (Nguyen et al., 2020). For the SAMI, a one-month lag is applied with the SAMI leading the ESI because the lagged relationship between the SAM and the ESI is stronger than with a

¹ $DMI = \overline{SST}(0 - 10^\circ S, 90 - 110^\circ E) - \overline{SST}(10^\circ S - 10^\circ N, 50 - 70^\circ E)$, where overbar denotes the area average.

² $EMI = \overline{SST}_{cp} - 0.5 * (\overline{SST}_{ep} + \overline{SST}_{wp})$, where cp denotes tropical central Pacific ($10^\circ S - 10^\circ N, 165 - 220^\circ E$), ep denotes tropical eastern Pacific ($15^\circ S - 5^\circ N, 250 - 290^\circ E$), and wp denotes tropical western Pacific ($10^\circ S - 20^\circ N, 125 - 145^\circ E$). The overbar represents the area average.

³ The AAO is obtained by projecting daily geopotential height anomalies at 700-hPa onto the leading mode of the EOF of the 700-hPa geopotential height variability over $20 - 90^\circ S$.

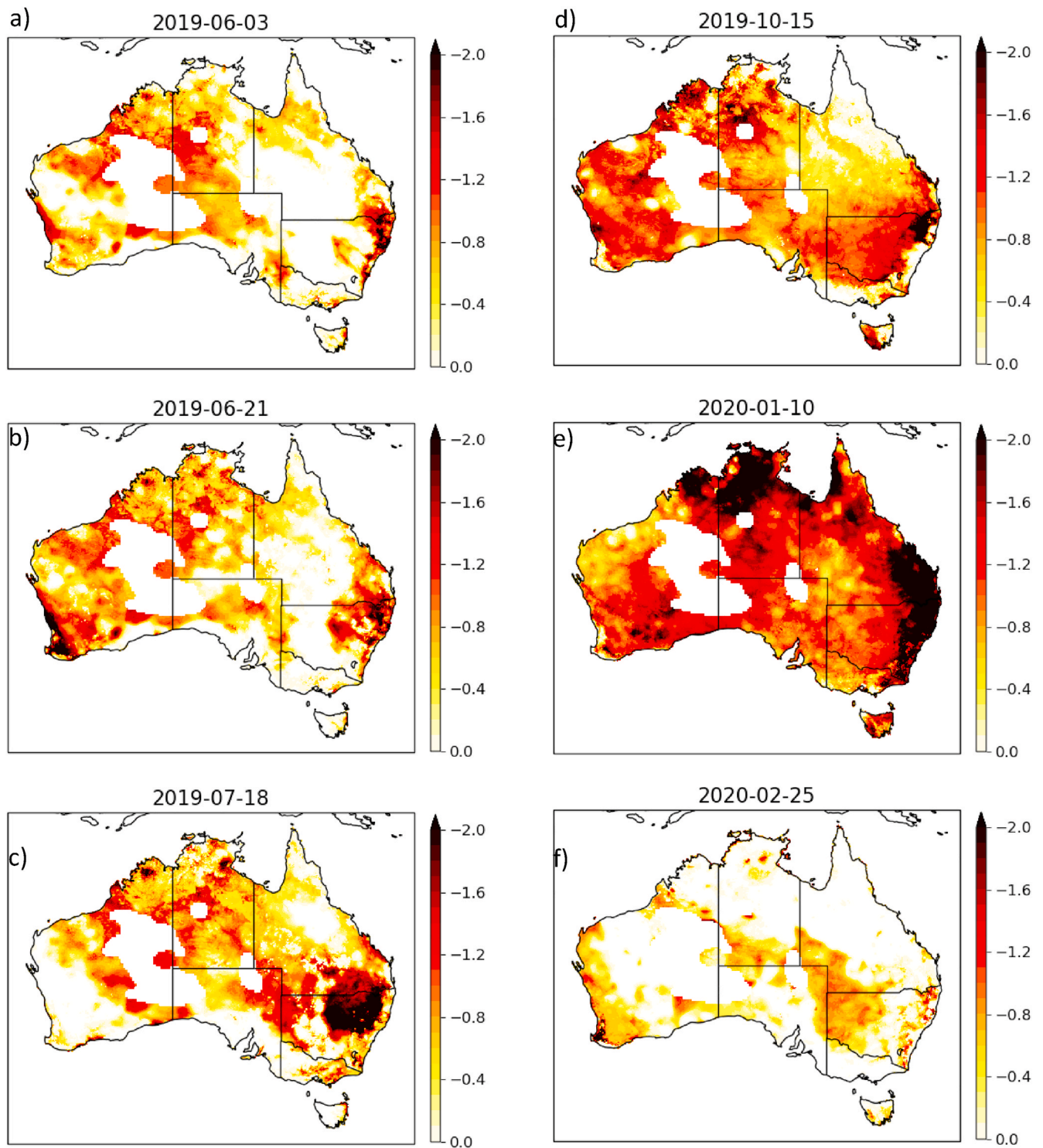


Fig. 4. Evolution of the 2019 flash drought sequence as depicted in the ESI from the beginning of (a) the rapid intensification ($t_{start}=3\text{-Jun-2019}$) to (f) the rapid recovery to normal conditions ($t_0=25\text{-Feb-2020}$). Only negative ESI values are shown. The other key dates are (b) $t_{onset}=21\text{-Jun-2019}$ and (c) $t_{min}=18\text{-Jul-2019}$. Two additional dates show a slight decrease of the ESI on (d) 15-Oct-2019 before peaking on the (e) 10-Jan-2020 as shown in Fig. 3.

zero-lag regression (Nguyen et al., 2020). The significance of the regression coefficients is assessed by using the analysis of variance and we impose $p\text{-value} = 0.01$ for the null hypothesis.

Note that neither rainfall nor temperature are used as predictors here because unlike the above climate modes, these variables especially rainfall may occur by chance through the chaotic nature of the weather and are not well predicted beyond about a week. Therefore, they will not provide potential predictability of the ESI on subseasonal to seasonal

time scale.

The period used to perform the multiple linear regression is limited by the availability of daily SST (1982–2018). The four regression coefficients obtained are then used to determine the projected values for a given selected date by multiplying each coefficient by the associated predictor value for the selected date. Hence, the resulting reconstructed ESI is the sum of the projected values from all four predictors, and the residual is the difference between the observed and reconstructed ESI

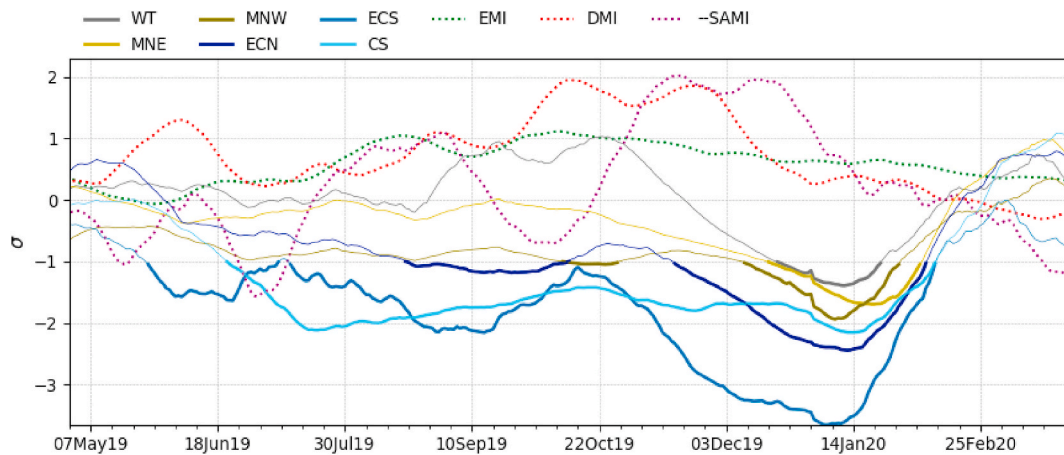


Fig. 5. Time series of the ESI averaged over NRM clusters (solid curves). Values below -1 are bold. Dotted curves are the standardized EMI (forest green), the DMI (red) and the SAMI (sign flipped, purple). The daily data are filtered with a 4-week running mean, with the indicated date corresponding to the last day of the window. Time marks are placed every 7 days. Positive anomalies of the dotted curves should likely correspond to negative anomalies of the solid curves. (For interpretation of the references to colour in this figure legend, the reader is referred to the Web version of this article.)

Table 1
The 2019 flash drought occurrence for 6 NRM clusters as defined in Fig. 1

cluster	Onset date (t_{onset})	End date (t_{end})	Duration (days)	Intensity (ESI)
CS	21-06-2019	10-02-2020	235	-1.73
ECS	16-11-2019	11-02-2020	88	-2.92
ECN	01-12-2019	07-02-2020	69	-2.00
WT	20-12-2019	23-01-2020	35	-1.23
MNE	25-12-2019	05-02-2020	43	-1.48
MNW	27-12-2019	29-01-2020	34	-1.64

(further details of this method can be found in Lim et al. (2021)).

Note that all variables used for the regression model are standardized and are 4-week running means with the same date convention as for the ESI. The regression is developed separately for each 4-week window during the year, taking data from up to 8 weeks earlier and later to each window. For example, the regression equation used for the 1st September window is generated using ESI and predictor data pairs from 7th July to 27th October. The use of data from 8 weeks earlier to 8 weeks later is required because of the lack of available number of years with which to compute a reliable regression – without doing this the regression coefficients become dominated by noise and are no longer a smoothly-varying function of the time of year. The effective degrees of freedom for each regression calculation is therefore 37 (the number of years) times 3 which is the number of non-overlapping 4-week windows in the period extending from minus 8 weeks to plus 8 weeks determined by the ESI autocorrelation coefficient below 0.36 (not shown).

3. Drought and flash drought inferred from the ESI

3.1. The 2017–2019 drought

The evolution and scale of the 2017–19 multi-year drought is depicted using the annual-mean ESI for 2016–2019 (Fig. 2). Conditions in 2016 were generally good for plant water supply, as indicated by positive ESI, across most of Australia. Following this more favourable year, a 3-year period of steadily worsening drought conditions commenced across eastern Australia, culminating in severe drought conditions in 2019.

The time series of area averaged ESI along with standardized anomalies of rainfall and temperature for the National Resource Management (NRM) cluster of regions called the Central Slopes (CS) are shown in Fig. 1b for the period 2016–2020. Cluster CS covers the north eastern quadrant of the MDB (Fig. 1a) and is indicative of what broadly

occurred elsewhere in subtropical eastern Australia. From late 2016 onward, rainfall and the ESI mostly remain below normal and temperature anomalies mostly above normal. Although there are 4 or 5 brief episodes where rainfall was above normal (e.g., Mar 2017, Oct 2017, Oct 2018, Mar 2019), the ESI dropped below zero at the beginning of 2018 and did not rise above zero again until Feb 2020. During the entire 2016–2020 period, positive temperature anomalies show high variability although they frequently attained values $> 2\sigma$, suggesting that the slow decline in ESI during 2017–2019 was driven more by persistently low rainfall.

Looking more closely at the ESI fluctuations in Fig. 1b, there were several sharp increases that lag by about one-month similar increases in rainfall. This shows that rainfall can quickly alleviate drought conditions, albeit temporarily. The ESI also exhibited several sharp declines, most notably in early 2019 and June 2019. After the latter, the ESI remained below -1 until Feb 2020. The sharp decline in June 2019 satisfies the flash drought criteria described in Sec. 2 and is further investigated below. These sharp declines in ESI occur during more sustained negative rainfall anomalies but coincide with brief episodes of very high temperature. This suggests a contribution of anomalously high temperatures for promoting the onset of flash drought. However, it should be noted that temperature only comes into the Penman equation for PET through the humidity term, so it is likely that wind, humidity, and radiation are also involved in flash drought onset.

During the 4-year period to the end of 2019, the overall trend in the ESI is negative with each peak and trough in the ESI falling below the previous one (Fig. 1b). This demonstrates the steadily worsening conditions during the drought. It also shows that ecological and agricultural drought may temporarily end or at least weaken, as represented by the occasional increases in the ESI, but then resumes after a few months. A likely explanation for the downward trend in ESI over the period, despite less obvious trends in temperature and rainfall, is the accumulative effect of the reduced rainfall and increased temperatures on the soil moisture and vegetation (e.g., Otkin et al., 2016).

The first instance of positive ESI over the most recent two years occurred at the end of February 2020, following heavy rainfall across eastern Australia (Fig. 1b). This rapid improvement marks the end of the 2017–2019 drought and is consistent with the “flash recovery” terminology introduced by Otkin et al. (2019) to describe the sudden transition from drought to above normal conditions. More details of the rapid declines in the ESI during 2019, i.e., flash drought, are given hereafter.

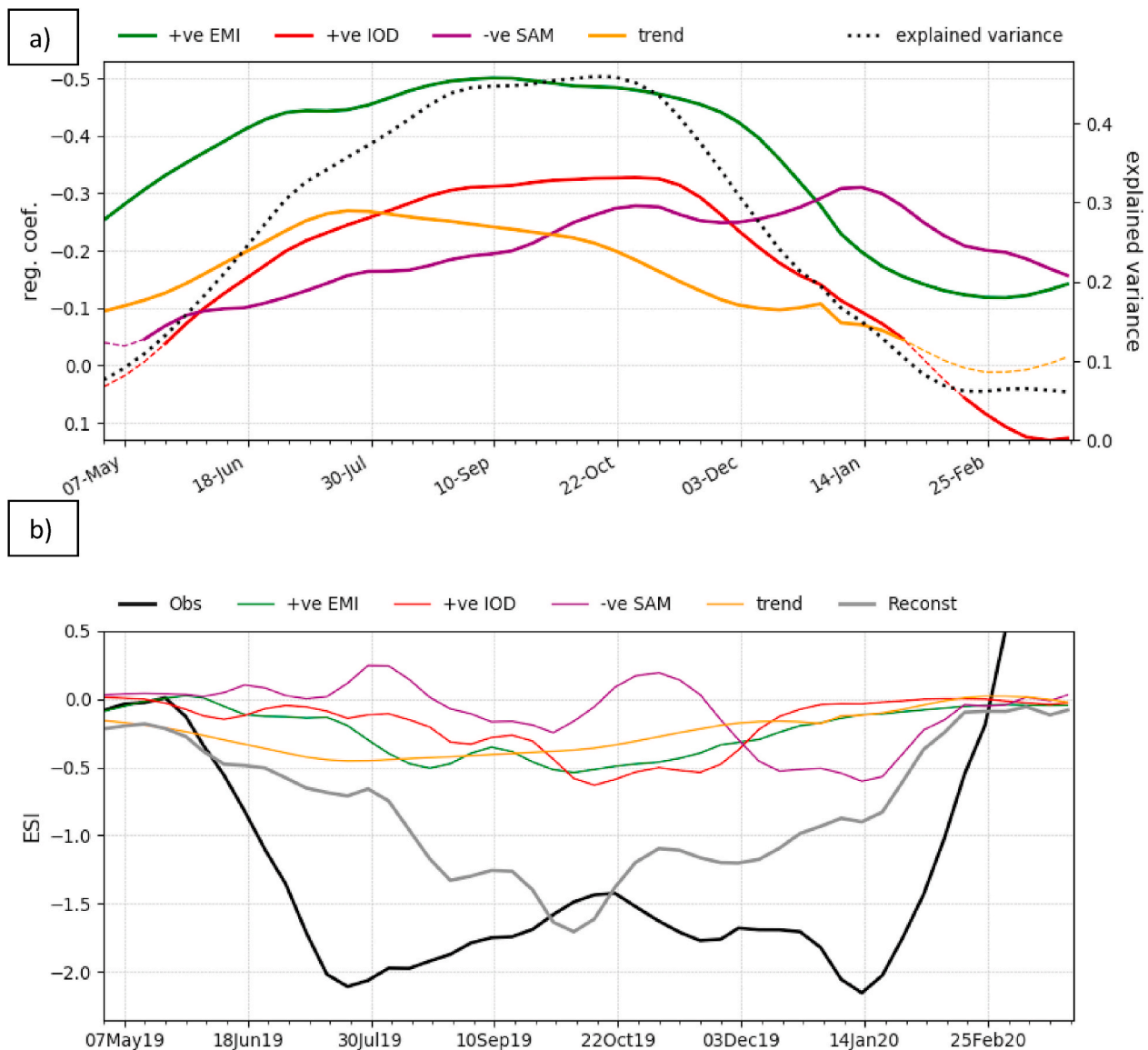


Fig. 6. (a) Time series of the ESI averaged over NRM cluster CS coefficients (left axis) regressed onto the detrended and standardized (i) EMI, (ii) DMI, (iii) 1-month lag reversed SAMI and (iv) linear trend centred on each 16-week period, calculated every week for the period 1982–2018. Values with p-value <0.01 are bold, they are dashed otherwise. The total variance explained is also indicated (dashed black line, right axis). (b) Time series of the ESI averaged over NRM cluster CS explained by the above 4 predictors using the multiple linear regression and scaled by the amplitude of the predictors at each date indicated on the x-axis. The reconstructed ESI using the multiple linear regression model (grey) and observed (black) ESI are also shown. Time marks are placed every 7 days.

3.2. The 2019 flash droughts

Following the method described in section 2, we objectively identify the flash droughts that occurred in Australia during 2019. Fig. 3 illustrates this objective identification for the example CS region (as identified in Fig. 1). The time series run from May 2019 to March 2020. The beginning of the rapid intensification period when $\delta ESI \leq p_{20}$ (i.e., bottom 20%) is defined as $t_{start}=3-Jun-2019$. The ESI first dropped below -1 on 21 June 2019, at which time $FDI=1$ ($\delta ESI \leq p_{20}$ for the previous 18 consecutive days and $ESI < -1$). Therefore, flash drought onset is flagged as $t_{onset}=21-Jun-2019$. The ESI continued to decrease from t_{onset} until it reached a local minimum on 18 July, which marks the end of the flash drought intensification period defined as $t_{min}=18-Jul-2019$. This drought event is defined to persist until the ESI increases to above -1 , which occurred on $t_{end}=10-Feb-2020$. The $t_0=25-Feb-2020$ indicates the moment $ESI = 0$ marking the return to normal conditions.

The flash drought event is then characterized by its duration $\Delta t = t_{end} - t_{onset}$ and its intensity $I = \overline{ESI}(t_{onset} : t_{end})$, where the overbar de-

notes the temporal average. A threshold is imposed to the length of any drought event to ensure that the event is impactful on agriculture such that $\Delta t \geq 4$ weeks.

Maps of the ESI across Australia for a sequence of key dates capturing the evolution of the flash drought event are shown in Fig. 4. At the beginning of the rapid intensification in the CS region, only a small portion of eastern Australia stretching along the east coast of New South Wales (NSW) is shown to be experiencing evaporative stress (Fig. 4a). By the flash drought onset date, an extended area of large negative $ESI < -1.2$ covering much of the cluster CS is evident (Fig. 4b). By the end of the intensification period, strong negative ESI well below -2 had formed in an area much larger than cluster CS (Fig. 4c). In comparison, on 15 October 2019 when drought conditions over the cluster CS had slightly weakened (Fig. 1b), the ESI (Fig. 4d) suggests that drought conditions extended across most of the country. After this, the ESI time series decreases again to its most extreme on 10 January 2020 (Fig. 1b) and the whole country is dominated by $ESI < -1$ and in the east and far north by $ESI < -2$ (Fig. 4e). At the end of February 2020 after the end of the flash

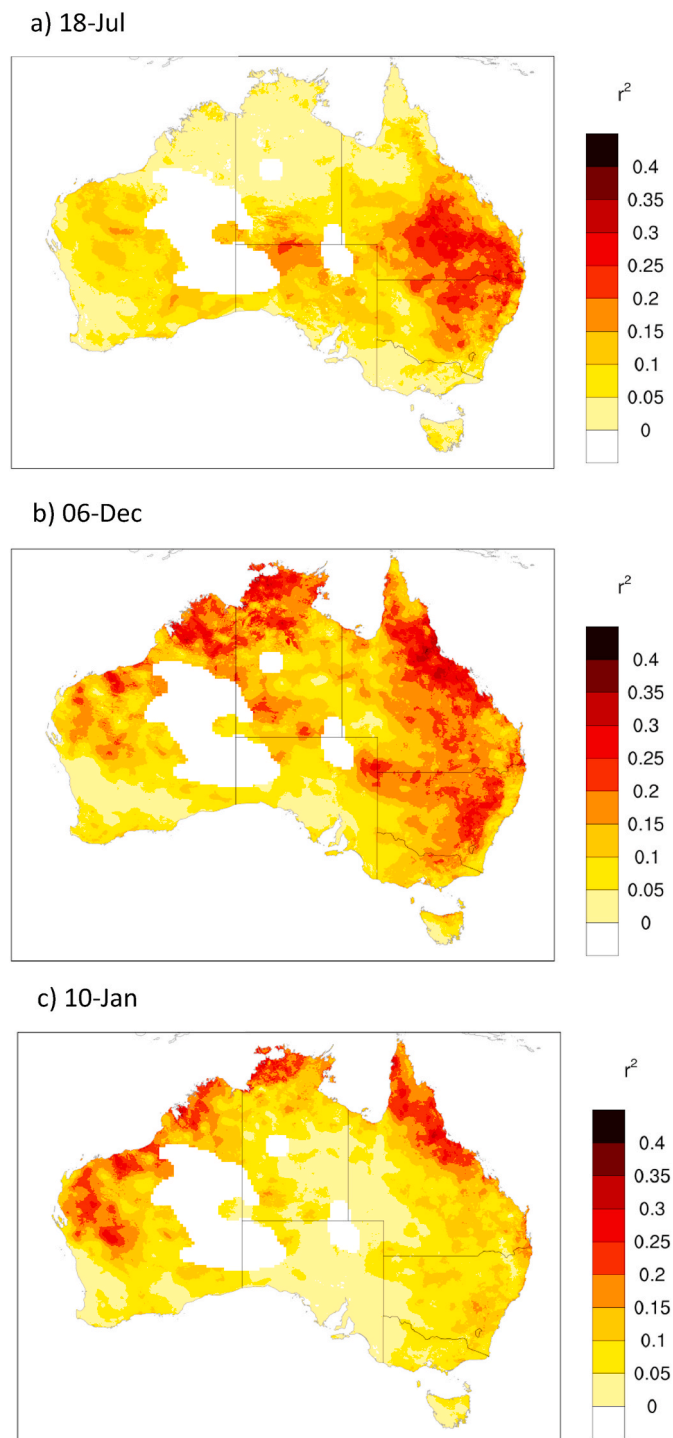


Fig. 7. ESI total variance explained by the four predictors EMI, DMI, 1-month lag SAMI and linear trend for the 16-week period centred on (a) 18 July, (b) 6 December and (c) 1 January over the years 1982–2018. The total variance includes only the regression coefficients with p -value < 0.01 .

drought, the ESI indicates near-normal conditions had returned across most of the country, marking the end of the multi-year drought event (Fig. 4f).

To further elucidate the rapid change of the ESI leading to intense negative values over northern and eastern Australia in January 2020, we show ESI time series for six NRM cluster regions in Fig. 5 (refer to Fig. 1 for the location of these clusters). These clusters were chosen because they each had an identified flash drought during 2019 whereas the other

clusters in Australia did not. All six clusters exhibit the strongest negative ESI around mid-January 2020. In contrast to cluster CS, the other clusters did not start their rapid change until November or December 2019, but all six clusters show the same flash recovery between late January and early February 2020. Applying the flash drought monitoring technique here, these clusters meet the criteria for the occurrence of a flash drought event, and their characteristics are summarized in Table 1. Although the CS event is the longest ($\Delta t = 235$ days), the East Coast South (ECS) is the most intense ($I = -2.92$). After the CS and ECS clusters, the next most severe flash drought was identified in the East Coast North (ECN) cluster with a duration of 69 days and intensity of -2 . Together the CS, ECS, and ECN regions occupy a large portion of subtropical eastern Australia, and we concentrate on these regions in the following analysis.

4. Role of climate drivers in the 2019 flash droughts

Nguyen et al. (2020) showed that on the seasonal time scale, the ESI over Australia is strongly correlated with the same climate drivers that affect Australian rainfall. In particular, the ESI tends to be more negative i) during El Niño throughout the entire year with the strongest signal in summer across the north and east; ii) during positive IOD in winter and spring across the south and east; and iii) during negative SAM in spring across the east. All three of these drivers are therefore relevant for drought in subtropical eastern Australia.

Here, we investigate the evolution of these drivers during the development of the 2019 flash droughts using the EMI, DMI and the inversely signed SAMI (Fig. 5). The EMI increased to about $+1\sigma$ in August 2019 and remained there until about mid-December, after which there was a slow decline until March 2020. The DMI was positive with a first peak of $+1.2\sigma$ in June 2019, then gradually increasing to $+2\sigma$ in October and remained around $+2\sigma$ for two months before declining to weakly negative values at the end of February 2020. The SAMI showed large variability during this period. The first peak of negative SAMI at about -1σ occurred around August 2019, but the second stronger peak of about -2σ occurred during November–December 2019.

In June 2019, the DMI peaked at $+1.2\sigma$ and EMI was weakly positive ($< +0.5\sigma$) while SAMI was positive (noting that the sign of SAMI is reversed in the purple dotted curve in Fig. 5). Between October and December 2019, not only did the positive DMI (peaking around $+2\sigma$) become stronger than in June, but both strong positive EMI (peaking at $+1.1\sigma$) and strong negative SAMI (peaking at -2.1σ) were present (Lim et al., 2021; Watterson, 2020). Strong negative SAMI resulted from the sudden stratospheric warming of September 2019 and was the strongest on record for the October to December season, playing a primary role in promoting high maximum temperatures, low rainfall, and an associated bushfire episode in eastern NSW in late spring 2019 (Lim et al., 2021; Bureau's Special Climate Statement 72, 73). This suggests that these large-scale oceanic and atmospheric circulations may have made significant contributions to the 2019 flash droughts.

To verify this hypothesis and quantify the contributions of these climate drivers, we perform a multiple linear regression on the ESI using these climate drivers as predictors. A linear trend is also included as a predictor to assess the role of the ongoing warming trend for this particularly strong flash drought event. Fig. 6a shows the ESI multiple linear regression coefficients for each of the four predictors EMI, DMI, SAMI and linear trend and the variance explained by the four predictors for cluster CS. These coefficients show that the impact of the trend maximises in winter, the impacts of ENSO and IOD maximise in late winter-spring while the impact of SAM maximises in summer. In terms of peak magnitude of the regression coefficients on any date, the order of importance of the predictors can be seen to be EMI, DMI, SAM, and lastly the trend, confirming our earlier statement that we did not expect a primary role for the trend. The explained variance of the CS ESI by the multiple regression peaks in spring at 0.46, suggesting that the ESI in this NRM cluster is most predictable in spring.

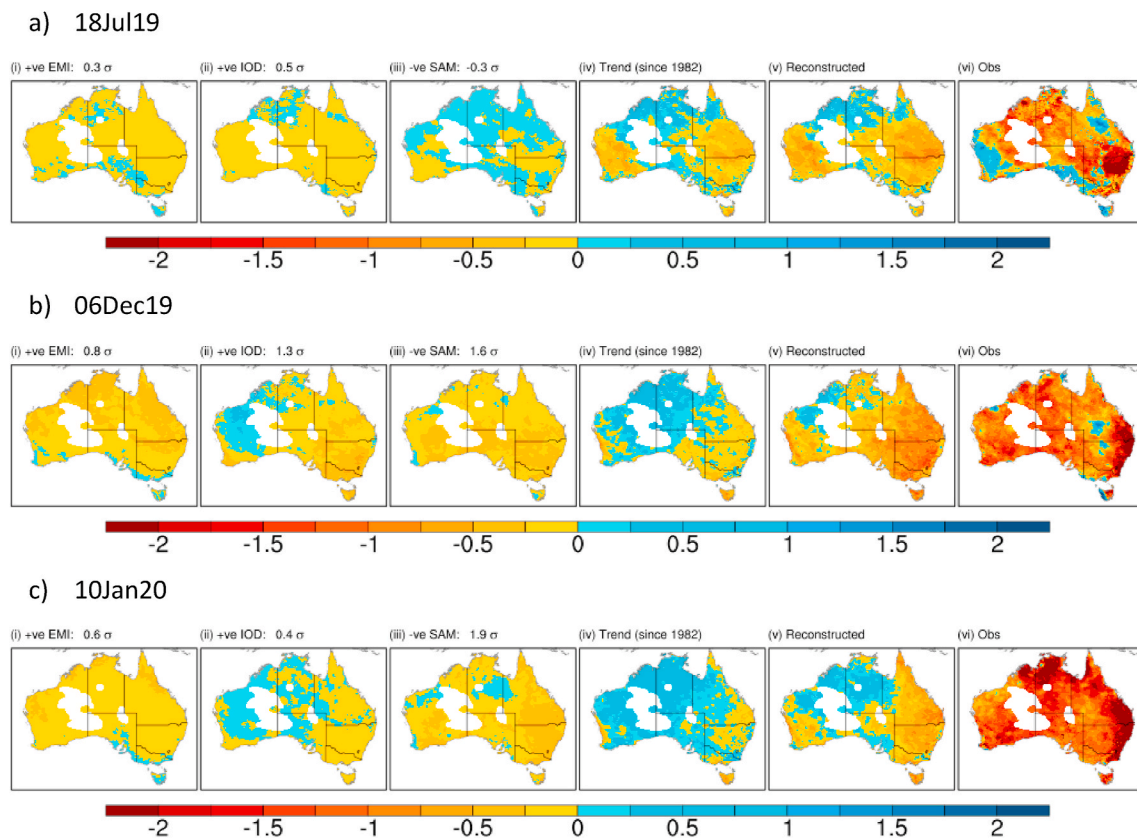


Fig. 8. ESI components reconstructed from the detrended and standardized (i) EMI, (ii) DMI, (iii) 1-month lag sign-reversed SAMI and (iv) the linear trend for (a) 18 July 2019, (b) 06 December 2019 and (c) 10 January 2020. The value on top of each panel indicates the magnitude of the predictors for each date. The total reconstructed ESI by the multiple linear regression is displayed in (v) and the observed ESI in (vi) of each date.

Using these multiple linear regression coefficients and the amplitudes of the predictors for each date, we obtain the time series of the ESI explained by each of the four predictors and the reconstructed ESI during 2019 and early 2020 (Fig. 6b). Prior to October 2019, all predictors contributed to the negative ESI except for the SAMI. After that, all predictors to the negative ESI, with the trend being least important. From a season-long perspective the reconstructed ESI during this period has some consistency with the observed ESI in that they are both negative during the winter to mid-summer. However, the reconstructed ESI fails to reproduce the sharp declines in the ESI in June 2019 and January 2020, the first of which was identified above as a flash drought. For the June 2019 flash drought onset, only about half the magnitude of the ESI decline was predicted by this linear regression model. It was only in October that the magnitude of the reconstructed ESI became equal, and slightly greater, than the observed, which further confirms the more predictable nature of the variability in spring in the region. By February, all regression coefficients returned to neutral followed by the ESI.

To generalise the impacts of these predictors across Australia, we apply the multiple linear regression to the ESI at each gridpoint to assess the extent the regression model above holds. Based on the flash drought sequence (Fig. 4) and the ESI evolution for cluster CS (Fig. 6b), here we reconstruct the ESI for the two dates of strongest negative ESI of 18 July 2019 and 10 January 2020. We also include the intermediate date 6 December 2019, which is around the onset dates of flash drought in the other NRM clusters (Table 1). We show maps of the explained variance on these dates for all years going into the regression (1982–2018, Fig. 7) along with the ESI components reconstructed for these three key dates in 2019/20 (Fig. 8). The variance explained by the four predictors for July varies between 0.2 and 0.35 in much of eastern Queensland and NSW, and especially in the flash drought affected area (compare with Fig. 4). The December explained variance also broadly matches the flash

drought affected areas in the east and north shown in Fig. 4. Note however that the coastal strip along NSW and Victoria has only a relatively low explained variance, which suggests that it will be difficult to account for much of the December 2019 flash drought in these coastal zones. This region is generally dominated by east coast lows that cause heavy rain events, which also have a weak relationship with these predictors (Dowdy et al., 2019). In January, most of the explained variance is located in the north-northwest.

Breaking down the effect of each predictor on the ESI in 2019/20 (Fig. 8), the ESI for the different predictors show similar features in subtropical eastern Australia to those seen in the CS time series (Fig. 6). In July, all four predictors display some contribution to the strong negative ESI in subtropical eastern Australia, with the linear trend showing the strongest contribution to the total reconstructed ESI. In contrast, in December all three modes of variability, Central Pacific El Niño, positive IOD and negative SAM significantly contribute to the strong negative ESI anomalies associated with the flash drought events in the ECN and ECS clusters while the linear trend shows a much smaller contribution. It appears that the Central Pacific El Niño contribution is mainly in the northern half of the country, the IOD dominates in the southwest and southeast, the negative SAM contributes most in the southern half of the country, and the trend contributes mainly over Tasmania. The amplitude of the predictors in December was much stronger than for July with November SAMI being strongest (-1.6σ). Despite these predictors' strengths, only about half the magnitude of the observed strongly negative ESI in subtropical eastern Australia in December could be explained by them.

Finally, in January 2020, while the amplitude of the SAMI increased compared to the previous month (-1.9σ), both the EMI and DMI decreased markedly. This is reflected in the reconstructed ESI which is well below the observed negative ESI across the country, making

January the least predictable by this linear regression model.

5. Conclusion

The recent multi-year drought across subtropical eastern Australia was the driest and hottest 3-year period since 1911. During 2017–2019, the drought impacts increased to become most severe in 2019 after several episodes of rapid intensification that we have objectively identified as flash drought. Flash drought developed first in the Central Slope region in conjunction with the positive IOD and Central Pacific El Niño Modoki from June 2019. This flash drought event further gained in intensity and additional flash droughts developed in the nearby East Coast North and East Coast South regions from late November under the influence of the combined effects of: (i) very strong positive IOD from October to December; (ii) moderately strong Central Pacific El Niño Modoki from October to November; and (iii) very strong negative SAM from November to December.

Through the monitoring of drought using the ESI, we show that the 2019 flash droughts can be detected and fully characterised in terms of their timing, duration and severity. The linear attribution suggests that at least during the 2019 spring season, the co-occurrence of strong positive IOD, El Niño-Modoki and strong negative SAM may have offered some predictability of the widespread drought conditions given that these climate modes are generally well predicted by both statistical and dynamical coupled multi-week to seasonal prediction systems (e.g. Hudson et al., 2017). However, the climate drivers alone could not predict the precise timing or magnitude of the local regions of flash drought. Useful prediction of flash drought will therefore require more local and current information than such large-scale climate drivers alone, such as may be provided by the atmospheric initial conditions in dynamical models. Current work is therefore underway to assess the flash drought predictability in the Australian Community Climate and Earth-System Simulator-Seasonal v1.0 (ACCESS-S1) model (Hudson et al., 2017).

Declaration of competing interest

The authors declare that they have no known competing financial interests or personal relationships that could have appeared to influence the work reported in this paper.

Acknowledgements

We warmly thank Andrew Dowdy and Andrew Watkins for their internal review and the two anonymous reviewers that helped significantly improve the manuscript. This work is supported by the Northern Australian Climate Program (NACP, <https://www.nacp.org.au/>), funded by Meat and Livestock Australia, the Queensland Government and the University of Southern Queensland. E.-P. Lim is supported by the Forewarned is Forearmed project funded by the Australian Government Department of Agriculture as part of its Rural R&D for Profit programme.

References

- Anderson, M.C., Hain, C., Otkin, J., Zhan, X., Mo, K., Svoboda, M., Wardlaw, B., Pimstein, A., 2013. An Intercomparison of drought indicators based on thermal remote sensing and NLDAS-2 simulations with U.S. Drought Monitor Classifications. *J. Hydrometeorol.* 14 (4), 1035–1056.
- Ashok, K., Behera, S.K., Rao, S.A., Weng, H., Yamagata, T., 2007. El Niño Modoki and its possible teleconnection. *J. Geophys. Res.* 112, C11007. <https://doi.org/10.1029/2006JC003798>.
- Cai, W., van Rensch, P., Cowan, T., Hendon, H.H., 2012. An asymmetry in the IOD and ENSO teleconnection pathway and its impact on Australian climate. *J. Clim.* 25, 6318–6329. <https://doi.org/10.1175/JCLI-D-11-00501.1>.
- Christian, J.I., Basara, J.B., Otkin, J.A., Hunt, E.D., Wakefield, R.A., Flanagan, P.X., Xiao, X., 2019. A methodology for flash drought identification in gridded datasets: application of flash drought frequency across the United States. *J. Hydrometeorol.* 20, 833–846.
- Dowdy, A.J., Pepler, A., Di Luca, A., et al., 2019. Review of Australian east coast low pressure systems and associated extremes. *Clim. Dynam.* 53, 4887–4910. <https://doi.org/10.1007/s00382-019-04836-8>.
- Frost, A.J., Ramchurn, A., Smith, A., 2018. The Australian landscape water balance model (AWRA-L v6). Tech.Descr.Aust.Water.Resour. Assess.Landscape model version.Bur.Meteorol.Tech. Rep. 1–58. http://www.bom.gov.au/water/landscape/assets/static/publications/AWRALv6_Model_Description_Report.pdf.
- Hudson, D., Coauthors, 2017. ACCESS-S1: the new Bureau of Meteorology multi-week to seasonal prediction system. *J. South. Hemisph. Earth Syst. Sci.* 673, 132–159. <https://doi.org/10.22499/3.6703.001>.
- Jones, D.A., Wang, W., Fawcett, R., 2009. High-quality spatial climate data-sets for Australia. *Aust. Meteorol. Oceanogr.* 58, 233–248.
- Khan, M.S., Baik, J., Choi, M., 2020. Inter-comparison of evapotranspiration datasets over heterogeneous landscapes across Australia. *Adv. Space Res.* 66 (3), 533–545. <https://doi.org/10.1016/j.asr.2020.04.037>.
- Lim, E.-P., Hendon, H.H., Boschhat, G., Hudson, D., Thompson, D.W.J., Dowdy, A.J., Arblaster, J.M., 2019. Australian hot and dry extremes induced by weakenings of the stratospheric polar vortex. *Nat. Geosci.* <https://doi.org/10.1038/s41561-019-0456-x>.
- Lim, E.-P., Hendon, H.H., Butler, A.H., Thompson, D.W.J., Lawrence, Z., Scaife, A.A., Shepherd, T.G., Polichtchouk, I., Nakamura, H., Kobayashi, C., Comer, R., Coy, L., Dowdy, A., Garreaud, R.D., Newman, P.A., Wang, G., 2021. The 2019 Southern Hemisphere stratospheric polar vortex weakening and its Impacts. *BAMS.* <https://doi.org/10.1175/BAMS-D-20-0112.1> (in print).
- Nguyen, H., Wheeler, M.C., Otkin, J.A., Cowan, T., Frost, A., Stone, R., 2019. Using the evaporative stress index to monitor flash drought in Australia. *Environ. Res. Lett.* 14, 064016.
- Nguyen, H., Otkin, J.A., Wheeler, M.C., Hope, P.K., Trewin, B., Pudmenzky, C., 2020. Climatology and variability of the evaporative stress index (ESI) and its suitability as a tool to monitor Australian droughts. *J. Hydrometeorol.* <https://doi.org/10.1175/JHM-D-20-0042.1> (in press).
- Otkin, J.A., Anderson, M.C., Hain, C., Svoboda, M., Johnson, D., Mueller, R., Tadesse, T., Wardlaw, B., Brown, J., 2016. Assessing the evolution of soil moisture and vegetation conditions during the 2012 United States flash drought. *Agric. For. Meteorol.* 218–219, 230–242.
- Otkin, J.A., Zhong, Y., Lorenz, D., Anderson, M.C., Hain, C., 2018a. Exploring seasonal and regional relationships between the Evaporative Stress Index and surface weather and soil moisture anomalies across the United States. *Hydrol. Earth Syst. Sci.* 22, 5373–5386.
- Otkin, J.A., Svoboda, M., Hunt, E.D., Ford, T.W., Anderson, M.C., Hain, C., Basara, J.B., 2018b. Flash droughts: a review and assessment of the challenges imposed by rapid onset droughts in the United States. *Bull. Am. Meteorol. Soc.* 99, 911–919.
- Otkin, J.A., Zhong, Y., Hunt, E.D., Basara, J., Svoboda, M., Anderson, M.C., Hain, C., 2019. Assessing the evolution of soil moisture and vegetation conditions during a flash drought–flash recovery sequence over the south-Central United States. *J. Hydrometeorol.* 20, 549–562. <https://doi.org/10.1175/JHM-D-18-0171.1>.
- Pendergrass, A.G., Meehl, G.A., Pulwarty, R., et al., 2020. Flash droughts present a new challenge for subseasonal-to-seasonal prediction. *Nat. Clim. Change* 10, 191–199. <https://doi.org/10.1038/s41558-020-0709-0>.
- Penman, H.L., 1948. Natural evaporation from open water, bare soil and grass. *The Royal Society* 193 (1032), 120–145. <https://doi.org/10.1098/rspa.1948.0037>.
- Reynolds, R.W., Smith, T.M., Liu, C., Chelton, D.B., Casey, K.S., Schlax, M.G., 2007. Daily high-resolution blended analyses for sea surface temperature. *J. Clim.* 20, 5473–5496. <https://doi.org/10.1175/2007JCLI1824.1>.
- Risbey, J.S., Pook, M.J., McIntosh, P.C., Wheeler, M.C., Hendon, H.H., 2009. On the remote drivers of rainfall variability in Australia. *Mon. Weather Rev.* 137, 3233–3253. <https://doi.org/10.1175/2009MWR2861.1>.
- Saji, N., Goswami, B., Vinayachandran, P., Yamagata, T., 1999. A dipole mode in the tropical Indian Ocean. *Nature* 401, 360–363. <https://doi.org/10.1038/43854>.
- Special Climate Statement 70, 2019. Drought conditions in Australia and impact on water resources in the Murray–Darling Basin. Bureau of Meteorology. <http://www.bom.gov.au/climate/current/statements/scs70b.pdf>.
- Special Climate Statement 72, 2019. Dangerous bushfire weather in spring 2019. *Bureau of Meteorology.* <http://www.bom.gov.au/climate/current/statements/scs72.pdf>.
- Special Climate Statement 73, 2020. Dangerous bushfire weather in spring 2019. *Bureau of Meteorology.* <http://www.bom.gov.au/climate/current/statements/scs73.pdf>.
- Wang, G., Hendon, H.H., 2007. Sensitivity of Australian rainfall to inter-El Niño variations. *J. Clim.* 20, 4211–4226. <https://doi.org/10.1175/JCLI4228.1>.
- Watterson, Ian., 2020. Australian Rainfall Anomalies in 2018–2019 linked to Indo-Pacific Driver indices using ERA5 reanalyses. *J. Geophys. Res. Atmos.* 125 (17), 19. <https://doi.org/10.1029/2020JD033041>.